ACS APPLIED NANO MATERIALS

www.acsanm.org Article

Au Nanoparticle Enhancement of Plasma-Driven Methane Conversion into Higher Order Hydrocarbons via Hot Electrons

Bofan Zhao, Indu Aravind, Sisi Yang, Yu Wang, Ruoxi Li, and Stephen B. Cronin*

Cite This: https://dx.doi.org/10.1021/acsanm.0c02912 Read Online

ACCESS | Metrics & More | Article Recommendations | Supporting Information

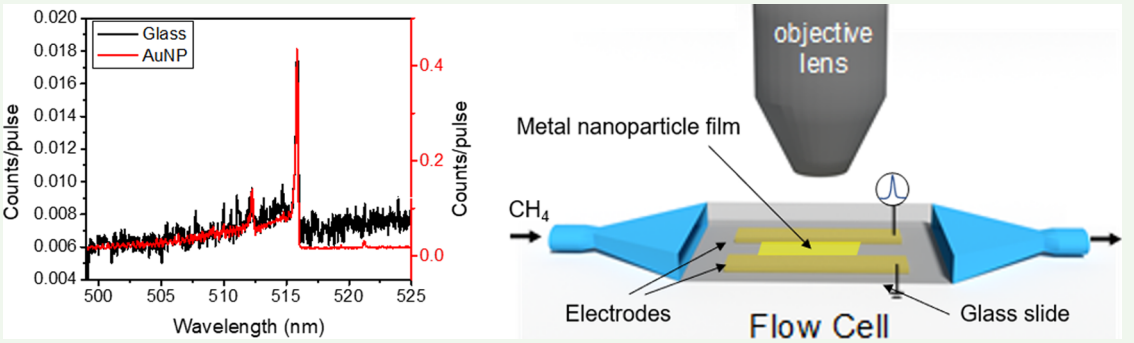

ABSTRACT: We demonstrate a more than 50-fold enhancement in the upconversion of methane to higher order hydrocarbons by discharging a nanosecond-pulsed plasma across Au nanoparticles. Here, the enhancement occurs as a result of the local field enhancement provided by the nanoparticles. The transient nature of the pulsed plasma enables the structure of these delicate nanoparticles to be preserved during the plasma discharge by producing a low-temperature plasma. Plasma emission spectroscopy shows signatures of the C_2 Swan bands with and without the presence of these nanoparticles. Mass spectrometry demonstrates that methane is converted into higher order hydrocarbons with different groups of peaks representing species with molecular masses of 35−45, 45−60, and 60−70 amu, corresponding to C_3, C_4, and C_5 species, respectively, under plasma discharge conditions. Electrostatic simulations show that a 3−4× enhancement in the field is produced at the nanoparticle surfaces. The exponential relation between electric field strength and plasma formation gives rise to a 50× increase in highly reactive, plasma-initiated radical species that are responsible for driving the methane upconversion process. This upconversion is important for several applications including mitigation of greenhouse emissions and improving the combustion of natural gas.

KEYWORDS: *plasma, nanosecond, methane conversion, greenhouse gasses, combustion*

INTRODUCTION

Due to the greenhouse effect and wide abundance of methane, conversion into other useful chemicals like syngas (CO and H_2) or higher order hydrocarbons has been pursued by many researchers.[1−5] However, the high dissociation energy of C−H bonds makes such conversion challenging and numerous methods, such as oxidative or nonoxidative catalytical reactions[6,7] and thermal coupling,[8] have been studied. Plasma discharges contain high-energy radical species that provide another approach for methane upconversion and reforming, which has been investigated using several different plasma generation techniques, including microwave plasma,[9] dielectric barrier discharge plasma,[10,11] and spark discharge.[12] However, methods to improve the efficiency and selectivity of this process are still very much needed in order to make this a viable approach for practical applications.

In addition to the mitigation of greenhouse gas emissions, the upconversion of methane to higher order hydrocarbons presents an important mechanism for enhancing the combustion of natural gas. While CH_4 is cheap, abundant, and relatively clean to burn, it has the highest ignition threshold and lowest burn rate among all *n*-alkanes (i.e., C_nH_{2n+2}), thus reducing its combustion robustness; a well-known problem in natural gas-burning systems. Several groups (including our own) have used transient plasma to enhance the ignition and burning of fuels that are present in natural gas, with CH_4 being the dominant one.[13−21] In contrast, C_2H_4 is one of the most readily combustible hydrocarbons due to its highly energetic C═C bond and its high diffusivity (i.e., relatively low molecular weight), and a stoichiometric C_2H_4/air flame burns twice as fast compared to a stoichiometric

Received: October 31, 2020
Accepted: November 23, 2020

https://dx.doi.org/10.1021/acsanm.0c02912
ACS Appl. Nano Mater. XXXX, XXX, XXX−XXX

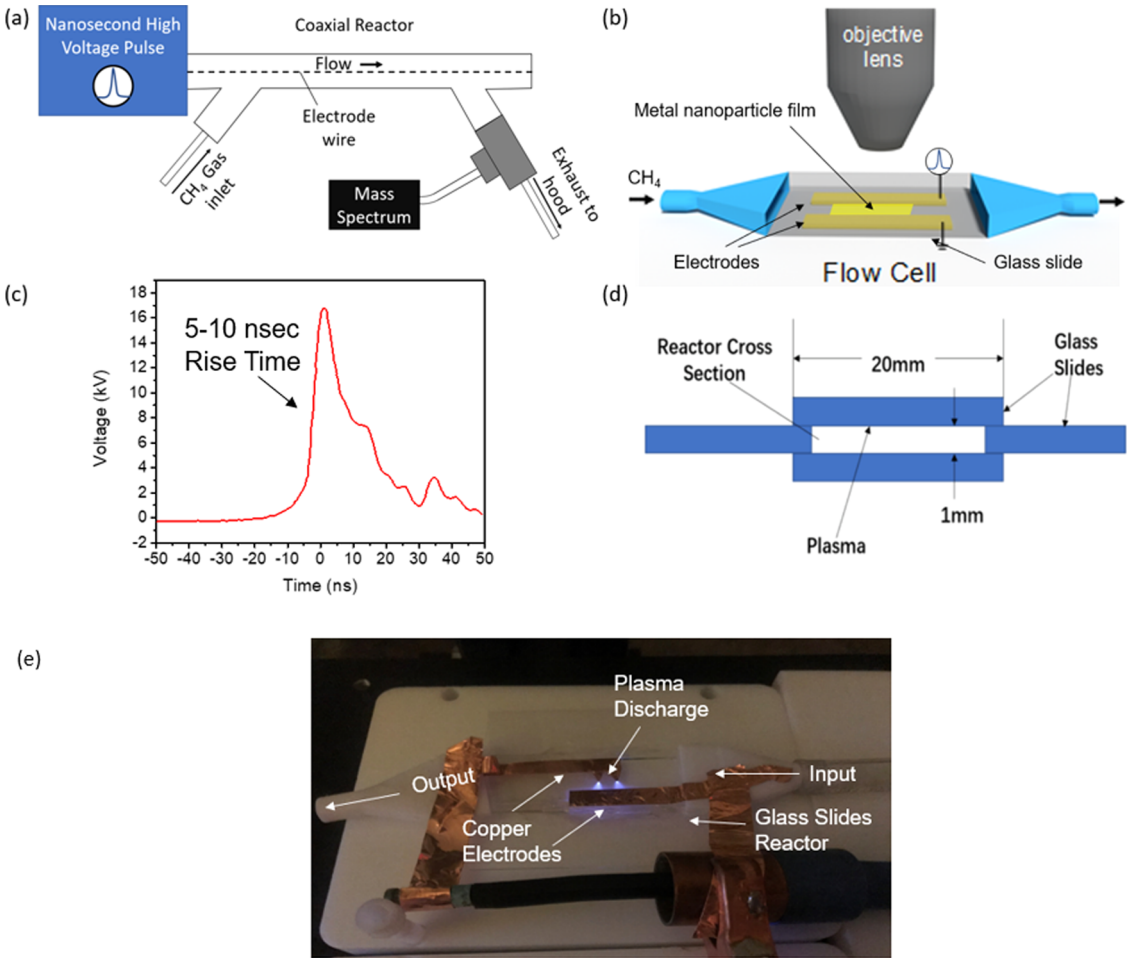

Figure 1. (a) Experimental setup of the coaxial reactor in which mass spectrometry data were taken. (b) Schematic diagram of a glass-slide reactor for plasma emission spectrum collection. (c) Typical waveform of a high-voltage pulse. (d) Cross-section and (e) real picture of a glass-slide reactor for our spectrum observation experiment.

CH_4/air flame. These prior investigations demonstrate that transient plasma can be used to achieve combustion under very lean fuel: air ratios, and hence lower greenhouse gas (GHG) emissions. However, the mechanism of this enhancement is not fully understood. The plasma-driven upconversion reported here presents one potential mechanism underlying this enhanced combustion of natural gas.

The formation of a plasma discharge consists of a series of several sequential processes, starting from electron emission, followed by acceleration and gas ionization, and ultimately leading to (and driving) chemical reactions.[22] Electron emission from discontinuous ultrathin metal films (i.e., nanoislands) has been studied as far back as 1962 by Neugebauer and Webb, who reported a deviation of electron conduction from Ohmic behavior on this kind of substrate.[23] The mechanism of electron emission from thin metal films was attributed to electric field emission at first.[24] However, later works on these discontinuous ultrathin metal films revealed the importance of the contribution of long-lifetime hot electrons, which have a relatively high probability to reach the nanoparticle surfaces in this process.[25−28] In addition, nanoscale sharp features, such as carbon nanotubes and semiconductor nanowires, have been known for their capability to enhance local electrostatic fields and, hence, field-emission of electrons.[29−34] Our group reported enhanced plasma emission spectra in Ar on metal nanoparticles due to this local field enhancement, and we have ruled out the possibility that such an enhancement originates from plasmon-resonant (i.e., optical) effects.[35]

In the work presented here, we explore the upconversion of methane to higher order hydrocarbons by discharging a nanosecond pulsed plasma across Au nanoparticles. This upconversion process is monitored using mass spectrometry and plasma emission spectroscopy. The local field enhancement provided by the nanoparticles underlying, which is responsible for the 50-fold enhancement of this process, is quantified using electrostatic simulations based on high-resolution transmission electron microscopy (HRTEM) images of the Au nanoparticles.

METHODS

Plasma is generated by a nanosecond high-voltage pulse (Figure 1c), which consumes far less energy in the creation of the plasma than conventional RF sources. The transient nature of the plasma necessitates that very little current is drawn in creating the plasma. Here, once the streamer is formed, the applied electric field drops to zero before a significant amount of current (or electric power) can flow. Furthermore, this transient plasma is more gentle to the delicate nanoparticles, as compared with conventional RF plasmas. The high-voltage pulses are produced by a pulse generator (SSPG-20X, Transient Plasma Systems, Inc.) with a rise time of 5−10 ns, as shown in Figure 1c. After gaseous molecules are ionized, the output voltage

https://dx.doi.org/10.1021/acsanm.0c02912
ACS Appl. Nano Mater. XXXX, XXX, XXX−XXX

drops quickly before a considerably large current flow can be formed, limiting the power that is drawn in the creation of this plasma.

These high-voltage nanosecond pulses are applied to a coaxial reactor with an inner electrode wire diameter of 0.025 in., an outer diameter of 1.5 in., and a length of 30 in., as illustrated in Figure 1a. Products from the reactor are then analyzed by mass spectrometry (Pieffer, GSD 301) to characterize products formed by discharging plasma in flowing CH_4. Figure 1b shows a photograph of a smaller reactor setup, referred to as a glass-slide flow reactor, which enables observation of plasma emission spectra, which consists of two copper electrodes separated by an approximately 5 mm gap inside a glass-slide flow reactor. We deposit nanoparticles using electron beam evaporation of metal films with a nominal thicknesses of 5−10 nm in between Cu electrodes, which are not thick enough to form continuous films and instead create island-like structures[36−38] The gas flow rate during these measurements was held constant at 100 sccm, while the plasma power spanned a range from 4.6 to 35 W for these measurements. Glass-slide reactors were also fabricated without Au nanoparticles as a comparison in order to evaluate the effect of nanoparticles. The plasma discharge observed in air (see Figure 1e) produces purple light that corresponds to the C−B transition in nitrogen.[39,40] The glass-slide-based reactor has a low profile and fits easily underneath our high numerical aperture microscope objective lens, enabling plasma emission spectra in the visible wavelength range to be obtained with high collection efficiency, as illustrated in Figure 1b. Based on the linear relationship between the C_2 Swan band emission and C_2 radical species concentration, as established by Goyette et al.,[41] we can use the Swan band spectral intensity as a proxy for CH_4 conversion.

RESULTS AND DISCUSSION

Figure 2 shows a comparison of the plasma emission spectra obtained in a CH_4 gas environment by discharging the nanosecond pulsed plasma both with and without nanoparticles. Here, copper electrodes are used both with and without nanoparticles deposited in between. We observe several sets of Swan bands, which correspond to C_2 (diatomic carbon) species[42,43] indicating that in addition to reducing CH_4 (i.e., a high barrier reaction), C_2-species are formed, presenting the exciting possibility of converting an abundant greenhouse gas into an energy-dense hydrocarbon fuel. Figure 2b shows the integrated area (i.e., plasma emission intensity) plotted as a function the nanosecond peak pulse voltage both with and without nanoparticles. At 9 kV, the plasma emission intensity obtained with nanoparticles is 50X larger than that obtained without nanoparticles. Below 9 kV, we only observe plasma emission with Au nanoparticles, indicating that enhancement factors much higher than this are created by the local field enhancement of the nanoparticles. In a previous study carried out in argon, enhancement factors of more than 1000-fold were observed with the presence of the nanoparticles.[35] Above 9 kV, the plasma emission is larger for the electrodes without nanoparticles, where the applied field is strong enough to initiate a plasma from the bulk electrodes. Here, the Au nanoparticle film creates a shunt of the externally applied field applied between the copper electrodes. Effectively, this film behaves as a conducting film at high voltages and an insulating film at low voltages.

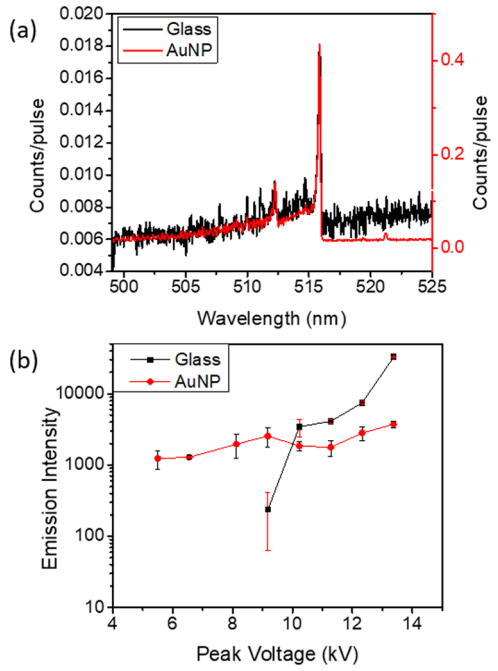

Figure 2. (a) CH_4 emission spectra (Swan band) on different substrates with and without Au nanoparticles and (b) their voltage dependence. Here, both configurations utilize copper electrodes. "Glass" refers to copper electrodes on a bare glass slide, whereas "AuNP" refers to the addition of Au nanoparticles deposited on the glass slide in between the copper electrodes.

Figure 3b shows the electric field enhancement observed on discontinuous Au nanoparticles in response to the nanosecond high-voltage pulse. Here, we performed quasi-static electromagnetic simulations using the COMSOL Multiphysics solutions package. The TEM image shown in Figure 3a is used to define the spatial extent of the Au nanoparticles. Floating boundary conditions were used in which the electric potential of each nanoparticle is freely varying. An extremely fine mesh (physics-optimized) was used to accurately model the short lengths over which electric fields decay near the nanoparticle surfaces. The electric field enhancement created by the Au nanoparticles is plotted in Figure 3b in response to an externally applied DC voltage. It should be noted that these are full 3D simulations, and we are plotting a 2D cross section in the plane of the glass surface. These simulations exhibit a

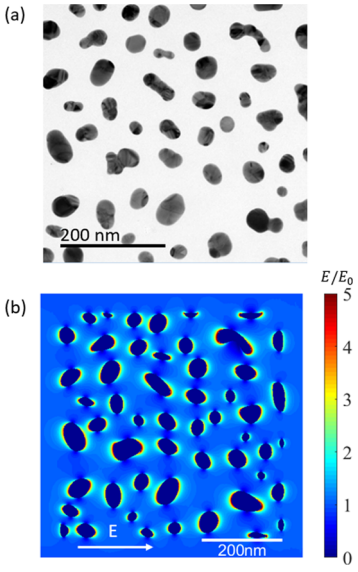

Figure 3. (a) HRTEM image of Au nanoparticles and (b) quasi-static simulations of the relative electric field enhancement produced by the Au nanoparticles.

https://dx.doi.org/10.1021/acsanm.0c02912
ACS Appl. Nano Mater. XXXX, XXX, XXX−XXX

three- to fourfold enhancement in the local electric fields on the nanoparticle surfaces. Since plasmas are generally initiated by field-emission of electrons which depends exponentially on the local *E*-field, this 3−4 fold increase in the local field can easily increase the plasma density by 50× under the same externally applied voltages, as observed in Figure 2b. Here, a quasi-static simulation was used to treat these nanosecond high-voltage pulses, which is justified because the timescale over which charge is redistributed in these metal nanoparticles is on the order of 50 fs. Therefore, the pulse rise time (i.e., 5 ns) is 5 orders of magnitude slower than this, justifying the use of the quasi-static simulations. Raman spectroscopy of the nanoparticles performed after plasma-driven methane conversion shows no peaks corresponding to carbon deposits (i.e., *D*-band or *G*-band). This indicates that there is no formation of coke, soot, or other carbonaceous deposits on the nanoparticles during the methane upconversion process.

Figure 4 shows the mass spectrometry data demonstrating the formation of C_3 (e.g., C_3H_8 (44 amu)), C_4 (e.g., C_4H_{10} (58 amu)), and C_5 (e.g., C_5H_{12} (70 amu)) hydrocarbon species under plasma excitation of CH_4. Here, we believe the formation of C_2 species, as observed by the Swan bands plotted in Figure 2a, plays an important role in the upconversion of these single C atom species to higher order hydrocarbons. Hydrogen is also detected in the product gases, as shown in Figure S4. The data shown in Figure 4 illustrate our ability to convert two abundant greenhouse gases CH_4 to higher order hydrocarbons that have a much higher energy density than methane. The reaction pathways of several related reactions (including the upconversion of methane) have been studied, proposing the initial formation of single carbon radicals, like CH_3 and CH_2, by the deprotonation of methane. Various combination pathways have been discussed to generate C_2 molecules and radicals, such as $CH_3 + CH_3 \rightarrow C_2H_6$ and $CH_3 + CH_2 \rightarrow C_2H_4 + H_2$. These C_2 radicals and molecules will further combine to produce longer hydrocarbon chains.[44−47] A summary of the potential reaction pathways can be found in Figure S5.

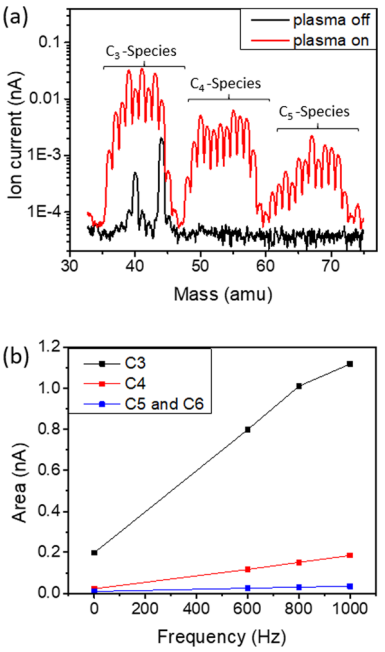

Figure 4. (a) Mass spectrometry data of a coaxial reactor (peaks near 40 and 44 are related to contaminations in the coaxial reactor and impurities from the gas line) and (b) its frequency dependence.

Figure 4b shows the integrated area in the mass spectra plotted as a function of the pulse repetition rate (i.e., frequency). Here, a linear relationship can be seen for all products within the tested frequency range. This result is not surprising since the plasma density is generally proportional to the pulse repetition rate.

Many difficult and interesting reactions have been driven by plasma (e.g., N_2 reduction with water to ammonia and CO_2 reduction to hydrocarbons). However, the main factor limiting the practical application/adoption of this approach is the lack of energy efficiency and prohibitively high voltages needed to initiate the plasma discharge. This nanoparticle-based approach enables these plasma-driven reactions to take place at lower voltages and potentially lower power (i.e., higher efficacies). Integral to this approach is the nanosecond pulses that preserve the integrity of the delicate nanoparticle nanostructures. Finally, this general approach ensures that the reaction takes place near the surface of the metal nanoparticles, which may open up a new avenue for catalyst-assisted plasma chemistry.

CONCLUSIONS

In conclusion, we demonstrate a more than 50-fold enhancement in methane upconversion to higher order hydrocarbons using a transient plasma discharged across an array of metal nanoparticles. Here, local field enhancement at the nanoparticle surfaces provides a mechanism for increasing the plasma discharge. Through this mechanism, plasma-driven chemical reactions can be enhanced or initiated under lower field conditions. Quasi-static electric field simulations are performed based on HRTEM images and predict local field enhancement factors of 3−4 fold near the nanoparticle surfaces. Since the plasma initiation depends exponentially on the peak electric field strength, this 3−4 fold increase in the local electric field strength can result in a more than one order-of-magnitude increase in the generation of plasma at a given applied external field strength. Due to the linear relationship between the C_2 Swan band emission intensity and C_2 radical productivity, we can conclude a similar enhancement in methane conversion into higher order hydrocarbons. This general approach can potentially be used to intentionally limit (or confine) plasma driven reactions to catalytic surfaces to improve catalytic selectivity.

ASSOCIATED CONTENT

Supporting Information

The Supporting Information is available free of charge at https://pubs.acs.org/doi/10.1021/acsanm.0c02912.

High-voltage pulse waveform; COMSOL simulation details; structure of the simulated sample; wider range of Swan band emission; gas chromatography result; and a potential reaction pathway in the reactor used for this study (PDF)

AUTHOR INFORMATION

Corresponding Author

Stephen B. Cronin − *Department of Physics and Astronomy and Ming Hsieh Department of Electrical Engineering, University of Southern California, Los Angeles, California*

https://dx.doi.org/10.1021/acsanm.0c02912
ACS Appl. Nano Mater. XXXX, XXX, XXX−XXX

90089, United States; Department of Chemistry, University of Southern California, Los Angeles, California 90089, United States; orcid.org/0000-0001-9153-7687; Email: scronin@usc.edu

Authors

Bofan Zhao − *Ming Hsieh Department of Electrical Engineering, University of Southern California, Los Angeles, California 90089, United States;* orcid.org/0000-0003-0478-6330

Indu Aravind − *Department of Physics and Astronomy, University of Southern California, Los Angeles, California 90089, United States*

Sisi Yang − *Department of Physics and Astronomy, University of Southern California, Los Angeles, California 90089, United States;* orcid.org/0000-0003-0352-833X

Yu Wang − *Mork Family Department of Chemical Engineering and Materials Science, University of Southern California, Los Angeles, California 90089, United States;* orcid.org/0000-0002-0307-1301

Ruoxi Li − *Mork Family Department of Chemical Engineering and Materials Science, University of Southern California, Los Angeles, California 90089, United States*

Complete contact information is available at: https://pubs.acs.org/10.1021/acsanm.0c02912

Notes

The authors declare no competing financial interest.

■ ACKNOWLEDGMENTS

This research was supported by the Army Research Office (ARO) award no. W911NF-19-1-0257 (B.Z.), the National Science Foundation (NSF) award no. CHE-1954834 (R.L.) and CBET-2012845 (I.A.), the Air Force Office of Scientific Research (AFOSR) grant no. FA9550-19-1-0115 (Y.W..), and the U.S. Department of Energy, Office of Basic Energy Sciences, award no. DE-SC0019322 (S.Y.).

■ REFERENCES

(1) Prettre, M.; Eichner, C.; Perrin, M. The catalytic oxidation of methane to carbon monoxide and hydrogen. *Trans. Faraday Soc.* **1946**, *42*, 335b−339b.

(2) Lunsford, J. H. Catalytic conversion of methane to more useful chemicals and fuels: a challenge for the 21st century. *Catal. Today* **2000**, *63*, 165−174.

(3) Wang, H. Y.; Ruckenstein, E. Conversions of Methane to Synthesis Gas over Co/γ-Al_2O_3 by CO_2 and/or O_2. *Catal. Lett.* **2001**, *75*, 13−18.

(4) Rostrup-Nielsen, J. R. Production of synthesis gas. *Catal. Today* **1993**, *18*, 305−324.

(5) Choudhary, V. R.; Rajput, A. M.; Rane, V. H. Low-temperature catalytic selective partial oxidation of methane to carbon monoxide and hydrogen over nickel/ytterbium sesquioxide. *J. Phys. Chem.* **1992**, *96*, 8686−8688.

(6) Nahreen, S.; Praserthdam, S.; Perez Beltran, S.; Balbuena, P. B.; Adhikari, S.; Gupta, R. B. Catalytic Upgrading of Methane to Higher Hydrocarbon in a Nonoxidative Chemical Conversion. *Energy Fuels* **2016**, *30*, 2584−2593.

(7) Lunsford, J. H. The catalytic conversion of methane to higher hydrocarbons. *Catal. Today* **1990**, *6*, 235−259.

(8) Rokstad, O. A.; Olsvik, O.; Holmen, A. Thermal Coupling of Methane. In *Studies in Surface Science and Catalysis*; Holmen, A.; Jens, K. J.; Kolboe, S., Eds.; Elsevier: 1991; Vol. *61*, pp. 533−539.

(9) Oumghar, A.; Legrand, J. C.; Diamy, A. M.; Turillon, N. Methane conversion by an air microwave plasma. *Plasma Chem. Plasma Process.* **1995**, *15*, 87−107.

(10) Zhang, Y.-p.; Li, Y.; Wang, Y.; Liu, C.-j.; Eliasson, B. Plasma methane conversion in the presence of carbon dioxide using dielectric-barrier discharges. *Fuel Process. Technol.* **2003**, *83*, 101−109.

(11) Zhou, L. M.; Xue, B.; Kogelschatz, U.; Eliasson, B. Partial Oxidation of Methane to Methanol with Oxygen or Air in a Nonequilibrium Discharge Plasma. *Plasma Chem. Plasma Process.* **1998**, *18*, 375−393.

(12) Shapoval, V.; Marotta, E. Investigation on Plasma-Driven Methane Dry Reforming in a Self-Triggered Spark Reactor. *Plasma Process. Polym.* **2015**, *12*, 808−816.

(13) Ombrello, T.; Qin, X.; Ju, Y.; Gutsol, A.; Fridman, A.; Carter, C. Combustion Enhancement via Stabilized Piecewise Nonequilibrium Gliding Arc Plasma Discharge. *AIAA J.* **2006**, *44*, 142−150.

(14) Starikovskii, A. Y.; Anikin, N. B.; Kosarev, I. N.; Mintoussov, E. I.; Starikovskaia, S. M.; Zhukov, V. P. Plasma-assisted Combustion. *Pure Appl. Chem.* **2006**, *78*, 1265−1298.

(15) Cathey, C.; Cain, J.; Wang, H.; Gundersen, M. A.; Carter, C.; Ryan, M. OH Production by Transient Plasma and Mechanism of Flame Ignition and Propagation in Quiescent Methane−air Mixtures. *Combust. Flame* **2008**, *154*, 715−727.

(16) Wolk, B.; Defilippo, A.; Chen, J.-Y.; Dibble, R.; Nishiyama, A.; Ikeda, Y. Enhancement of Flame Development by Microwave-assisted Spark Ignition in Constant Volume Combustion Chamber. *Combust. Flame* **2013**, *160*, 1225−1234.

(17) Wu, L.; Lane, J.; Cernansky, N. P.; Miller, D. L.; Fridman, A. A.; Starikovskiy, A. Y. Plasma-assisted Ignition below Self-ignition Threshold in Methane, Ethane, Propane and Butane-air Mixtures. *Proc. Combust. Inst.* **2011**, *33*, 3219−3224.

(18) Fei, W.; Liu, J. B.; Sinibaldi, J.; Brophy, C.; Kuthi, A.; Jiang, C.; Ronney, P.; Gundersen, M. A. Transient Plasma Ignition of Quiescent and Flowing Air/Fuel Mixtures. *IEEE Trans. Plasma Sci.* **2005**, *33*, 844−849.

(19) Rao, X.; Hammack, S.; Lee, T.; Carter, C.; Matveev, I. B. Combustion Dynamics of Plasma-Enhanced Premixed and Non-premixed Flames. *IEEE Trans. Plasma Sci.* **2010**, *38*, 3265−3271.

(20) Yin, Z.; Montello, A.; Carter, C. D.; Lempert, W. R.; Adamovich, I. V. Measurements of Temperature and Hydroxyl Radical Generation/decay in Lean Fuel−air Mixtures Excited by a Repetitively Pulsed Nanosecond Discharge. *Combust. Flame* **2013**, *160*, 1594−1608.

(21) Shukla, B.; Gururajan, V.; Eisazadeh-Far, K.; Windom, B.; Singleton, D.; Gundersen, M. A.; Egolfopoulos, F. N. Effects of Electrode Geometry on Transient Plasma Induced Ignition. *J. Phys. D: Appl. Phys.* **2013**, *46*, 205201.

(22) Piel, A.; Piel, A. *Stochastic Processes in a Plasma*, 2010; pp. 73−106.

(23) Neugebauer, C. A.; Webb, M. B. Electrical Conduction Mechanism in Ultrathin, Evaporated Metal Films. *J. Appl. Phys.* **1962**, *33*, 74−82.

(24) Dittmer, G. Electrical conduction and electron emission of discontinuous thin films. *Thin Solid Films* **1972**, *9*, 317−328.

(25) Borziak, P. G.; Kulyupin, Y. A.; Nepijko, S. A.; Shamonya, V. G. Electrical conductivity and electron emission from discontinuous metal films of homogeneous structure. *Thin Solid Films* **1981**, *76*, 359−378.

(26) Borziak, P. G.; Kulyupin, Y. A. Investigations of discontinuous metal films in the U.S.S.R. *Thin Solid Films* **1977**, *44*, 1−19.

(27) Borziak, P.; Kulyupin, Y.; Tomchuk, P. Electron processes in discontinuous metal films. *Thin Solid Films* **1975**, *30*, 47−53.

(28) Fedorovich, R. D.; Naumovets, A. G.; Tomchuk, P. M. Electron and light emission from island metal films and generation of hot electrons in nanoparticles. *Phys. Rep.* **2000**, *328*, 73−179.

(29) Wang, Q. H.; Corrigan, T. D.; Dai, J. Y.; Chang, R. P. H.; Krauss, A. R. Field emission from nanotube bundle emitters at low fields. *Appl. Phys. Lett.* **1997**, *70*, 3308−3310.

(30) Bonard, J. M.; Salvetat, J. P.; Stöckli, T.; de Heer, W. A.; Forró, L.; Châtelain, A. Field emission from single-wall carbon nanotube films. *Appl. Phys. Lett.* **1998**, *73*, 918−920.
(31) Zhu, W.; Bower, C.; Zhou, O.; Kochanski, G.; Jin, S. Large current density from carbon nanotube field emitters. *Appl. Phys. Lett.* **1999**, *75*, 873−875.
(32) Zhu, Y. W.; Zhang, H. Z.; Sun, X. C.; Feng, S. Q.; Xu, J.; Zhao, Q.; Xiang, B.; Wang, R. M.; Yu, D. P. Efficient field emission from ZnO nanoneedle arrays. *Appl. Phys. Lett.* **2003**, *83*, 144−146.
(33) Lee, C. J.; Lee, T. J.; Lyu, S. C.; Zhang, Y.; Ruh, H.; Lee, H. J. Field emission from well-aligned zinc oxide nanowires grown at low temperature. *Appl. Phys. Lett.* **2002**, *81*, 3648−3650.
(34) Fang, X.; Bando, Y.; Gautam, U. K.; Ye, C.; Golberg, D. Inorganic semiconductor nanostructures and their field-emission applications. *J. Mater. Chem.* **2008**, *18*, 509−522.
(35) Zhao, B.; Aravind, I.; Yang, S.; Cai, Z.; Wang, Y.; Li, R.; Subramanian, S.; Ford, P.; Singleton, D. R.; Gundersen, M. A.; Cronin, S. B. Nanoparticle-Enhanced Plasma Discharge Using Nanosecond High-Voltage Pulses. *J. Phys. Chem. C* **2020**, *124*, 7487−7491.
(36) Kumar, R.; Zhou, H.; Cronin, S. B. Surface-enhanced Raman spectroscopy and correlated scanning electron microscopy of individual carbon nanotubes. *Appl. Phys. Lett.* **2007**, *91*, 223105.
(37) Kneipp, K.; Kneipp, H.; Corio, P.; Brown, S. D. M.; Shafer, K.; Motz, J.; Perelman, L. T.; Hanlon, E. B.; Marucci, A.; Dresselhaus, G.; Dresselhaus, M. S. Surface-enhanced and normal Stokes and anti-Stokes Raman spectroscopy of single-walled carbon nanotubes. *Phys. Rev. Lett.* **2000**, *84*, 3470−3473.
(38) Liu, Z.; Hou, W.; Pavaskar, P.; Aykol, M.; Cronin, S. B. Plasmon Resonant Enhancement of Photocatalytic Water Splitting Under Visible Illumination. *Nano Lett.* **2011**, *11*, 1111.
(39) Saber, I.; Bartnik, A.; Skrzeczanowski, W.; Wachulak, P.; Jarocki, R.; Fiedorowicz, H.; Limpouch, J. Experimental and theoretical study on emission spectra of a nitrogen photoionized plasma induced by intense EUV pulses. *EPJ Web Conf.* **2018**, *167*, No. 03006.
(40) Zhang, Q. Y.; Shi, D. Q.; Xu, W.; Miao, C. Y.; Ma, C. Y.; Ren, C. S.; Zhang, C.; Yi, Z. Determination of vibrational and rotational temperatures in highly constricted nitrogen plasmas by fitting the second positive system of N_2 molecules. *AIP Adv.* **2015**, *5*, No. 057158.
(41) Goyette, A. N.; Lawler, J. E.; Anderson, L. W.; Gruen, D. M.; McCauley, T. G.; Zhou, D.; Krauss, A. R. Swan band emission intensity as a function of density. *Plasma Sources Sci. Technol.* **1998**, *7*, 149−153.
(42) Zeng, Y.; Tu, X. Plasma-Catalytic CO_2 Hydrogenation at Low Temperatures. *IEEE Trans. Plasma Sci.* **2016**, *44*, 405−411.
(43) Nicholls, R. W. The Interpretation of Intensity Distributions in the CN Violet, C_2 Swan, OH Violet and O_2 Schumann-Runge Band Systems by use of theirr-Centroids and Franck-Condon Factors. *Proc. Phys. Soc. A* **1956**, *69*, 741−753.
(44) Heijkers, S.; Aghaei, M.; Bogaerts, A. Plasma-Based CH4 Conversion into Higher Hydrocarbons and H2: Modeling to Reveal the Reaction Mechanisms of Different Plasma Sources. *J. Phys. Chem. C* **2020**, *124*, 7016−7030.
(45) Herrebout, D.; Bogaerts, A.; Yan, M.; Gijbels, R.; Goedheer, W.; Dekempeneer, E. One-dimensional fluid model for an rf methane plasma of interest in deposition of diamond-like carbon layers. *J. Appl. Phys.* **2001**, *90*, 570−579.
(46) Tachibana, K.; Nishida, M.; Harima, H.; Urano, Y. Diagnostics and modelling of a methane plasma used in the chemical vapour deposition of amorphous carbon films. *J. Phys. D: Appl. Phys.* **1984**, *17*, 1727−1742.
(47) Scapinello, M.; Delikonstantis, E.; Stefanidis, G. D. The panorama of plasma-assisted non-oxidative methane reforming. *Chem. Eng. Process.: Process Intesif.* **2017**, *117*, 120−140.

https://dx.doi.org/10.1021/acsanm.0c02912
ACS Appl. Nano Mater. XXXX, XXX, XXX−XXX